sciendo

PRODUCTION ENGINEERING ARCHIVES 2023, 29(4), 444-451

PRODUCTION ENGINEERING ARCHIVES

ISSN 2353-5156 (print)
ISSN 2353-7779 (online)

Exist since 4th quarter 2013
Available online at https://pea-journal.eu

Experimental-numerical analysis of the fracture process in smooth and notched V specimens

Grzegorz Świt[1*], Ihor Dzioba[2], Małgorzata Ulewicz[3], Sebastian Lipiec[2], Anna Adamczak-Bugno[1], Aleksandra Krampikowska[1]

[1] Faculty of Civil Engineering and Architecture, Kielce University of Technology, Av. 1000-an. of Polish State 7, 25-314 Kielce, Poland; gswit@tu.kielce.pl (GŚ); aadamczak@tu.kielce.pl (AAB); akramp@tu.kielce.pl (AK)
[2] Faculty of Mechatronics and Mechanical Engineering, Kielce University of Technology, Av. 1000-an. of Polish State 7, 25-314 Kielce; pkmid@tu.kielce.pl (ID); slipiec@tu.kielce.pl (SL)
[3] Faculty of Civil Engineering, Czestochowa University of Technology, 69 Dabrowskiego street, 42-201 Czestochowa; malgorzata.ulewicz@pcz.pl
*Correspondence: aadamczak@tu.kielce.pl

Article history
Received 20.07.2023
Accepted 18.10.2023
Available online 30.10.2023

Keywords
Pipelines
Finite element method
Stress
Strain
Tresca criterion

Abstract
This paper presents the outcomes of quality tests conducted on specimens, both smooth and V-notched, subjected to uniaxial tension, which were extracted from a gas transport pipeline. The introduction of the V-notch introduced variations in the stress and strain component fields near the plane of maximum constriction, consequently leading to their failure through different mechanisms. The process included the implementation of quality management practices such as numerical modeling and simulation of the loading of the specimens using ABAQUS. The material model employed in these calculations was defined and verified to ensure quality control. Subsequent to the numerical calculations, maps of the stress and strain component fields were generated, contributing to the quality assessment of the specimens. It was determined that the quality management process for the smooth specimen identifies the initiation of failure primarily due to the normal stress component in the central region of the plane with the largest constriction. In contrast, in the V-notched specimen, quality management efforts revealed that failure initiation occurs due to the tangential stress component, and failure proceeds through the shear mechanism. These results are valuable in developing a quality-driven methodology for monitoring the operational safety of gas network pipelines, primarily based on the analysis of acoustic emission signals.

DOI: 10.30657/pea.2023.29.49

1. Introduction and literature review

Of predominant importance for ensuring the safety of transmission of the medium and the economic aspect of maintenance of the gas infrastructure is, performed as part of maintenance work, the diagnostics of the technical condition of gas pipelines. An important part of the broader management of gas transport networks is to know the current condition of the pipeline material after a given period of operation. An accurate determination of the technical condition of the pipeline makes it possible to avoid costly and unnecessary stoppages in gas transport and unjustified replacements of pipe components (Zhao et al., 2002, Sharma et al., 2021).

Practice shows that it is impossible to achieve safe and long-term operation of linear pressure infrastructure without having reliable information about their actual condition. However, in order to properly assess the condition of a component, it is necessary to know the processes that affect the reduction in service life during its operation, to know the damage mechanisms and to be aware of the varying intensity of their occurrence under different operating conditions. Properly planned testing, prevention and condition monitoring carried out on the basis of the most up-to-date engineering knowledge are therefore essential. It should also be borne in mind that the diagnosis and assessment of the technical condition of gas pipelines should be carried out according to a structured system in which the type and extent of testing are a logical consequence of the analysis carried out (Zhao et al., 2002).

The primary objectives for the diagnostic system are to assess the actual technical condition and to determine the

prospects for further safe operation, including outlining the direction of possible upgrades to extend the life of the equipment. Diagnostic testing should be closely linked to forecasting, so it requires the selection of testing methods that, in addition to determining the actual condition at a given point in time, also offer the possibility of predicting the material behavior of components (Gumen et al., 2021; Parlak and Yavasoglu, 2023, Kosiń and Pawłowski, 2017, Piątkowski et al., 2020) over a relatively long period of further operation, under given operating conditions. Comprehensive testing methods can be used to determine the condition of a gas pipeline (Świt et al., 2022).

This paper proposes the implementation of a hybrid approach to the analysis of gas pipeline material: complementing the experimental results with the results of numerical simulations. The implementation of numerical simulations allows the determination of stress distributions, strains, stress triaxiality factor in the analyzed gas pipeline material, even after a certain period of operation. The numerical simulation method can solve any case with any geometrical conditions and any boundary conditions, using the computing power of computers (Alzyod and Ficzere 2023, Castillo et al., 2021; Karkowski and Grondys, 2021; Bokůvka et al., 2018; Fan et al., 2023, Bokůvka et al., 2018; Benhamena et al., 2023). The results of numerical simulations are within the limits of engineering accuracy. On the basis of the numerical results obtained, it is possible to develop conditions (criteria) to approximate under which circumstances a stress state will occur in the material. The proposed research methodology is in line with the local way of describing material destruction - taking into account the size distributions of the mechanical fields in the areas of the material with the highest strain.

Numerical analyses are increasingly used in the field of gas infrastructure research. Starting from the essence of the crack growth phenomenon, Misawa (Misawa et al., 2011) established a mathematical model of underground pipeline crack growth based on specific experimental data, which allows iterative calculations of pipeline deformation and crack growth. Song and Belytschko (Song and Belytschko, 2009) simulated the cracking and crack propagation process of a thin-walled cylindrical shell under internal explosive loading using an extended finite element method, which has good agreement with experimental results. Mitsuya (Mitsuya et al., 2013) calculated the dynamic stress intensity factor in crack propagation using the finite element method, obtaining the stress distribution in the region near the crack tip. Fonzo (Fonzo et al., 2006) simulated a full-scale blast experiment, the development of high-pressure tubes with internal air. Yang Xiao-Bin (Xiaobin et al., 2008), based on three linear pressure modes, investigated the dynamic expansion of a rich gas pipeline rupture using a finite element computational model. Shuai Jian (Jian et al., 2004) established a finite element model for dynamic pipeline rupture elongation and simulated the rupture using knot release technology.

This paper presents an experimental-numerical analysis of the fracture process of smooth and sharp-notched specimens taken from a gas transport pipeline. The aim of this research was to determine the failure mechanism of the specimen depending on the stress-strain field present. The research presented here is the first part of a study carried out to develop a method for monitoring the metal condition of gas pipelines based on the analysis of acoustic emission signals.

2. Materials and testing methods

In this study, specimens from steel taken from a gas transport pipeline were tested. The steel was characterized by a ferritic-pearlitic microstructure with a grain size of 7 - 12 μm (Fig. 1). In the microstructure image, structural banding, characteristic of structural steels in the normalized state, can be observed.

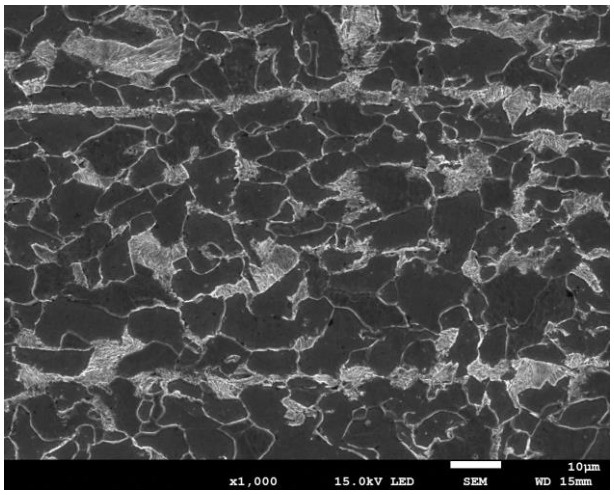

Fig. 1. Ferritic-perlitic microstructure of the analysed steel (x1000)

The material's strength and plasticity characteristics were determined by uniaxial tensile testing. The tests were carried out in accordance with PN-EN and ASTM standards (ASTM E8 / E8M-16ae1, 2016; PN-EN ISO 6892-1:2020-05, 2019). The tests were carried out at +20°C on a UTS/Zwick 100 testing machine, equipped with automated control and data recording systems. Specimens were loaded to failure. During the test, the force signal F and the elongation of the measuring part of the specimen u_{ext} were recorded. An extensometer with a measuring base of 25 mm and a resolution of 0.001 mm was used to record the elongation signal of the specimen. Based on the data obtained for the smooth specimen, the strength and yield characteristics of the steel analyzed were determined (Table 1). The nominal and true stress-strain relationships are shown in Figure 2a.

In order to comparatively analyze the influence of the stress and strain field distributions, specimens containing a V-notch were additionally tested (Fig. 2b). The diagrams of the specimens and the force-displacement relationships are shown in Fig. 2b. The influence of the notch on the load curves can be seen in the diagrams. The introduction of the notch on the specimen resulted in an increase in the level of the maximum loading force and a significant reduction in the elongation value.

Table 1. Strength and plasticity characteristics of the analysed steel

Charact.	$\sigma_{YS\_L}/\sigma_{YS\_H}$ [MPa]	σ_{UTS} [MPa]	E [GPa]	A_5 [%]	Z [%]
nominal	384/395	520.71	199	27.30	71.24
true	390/400	613.10	200		

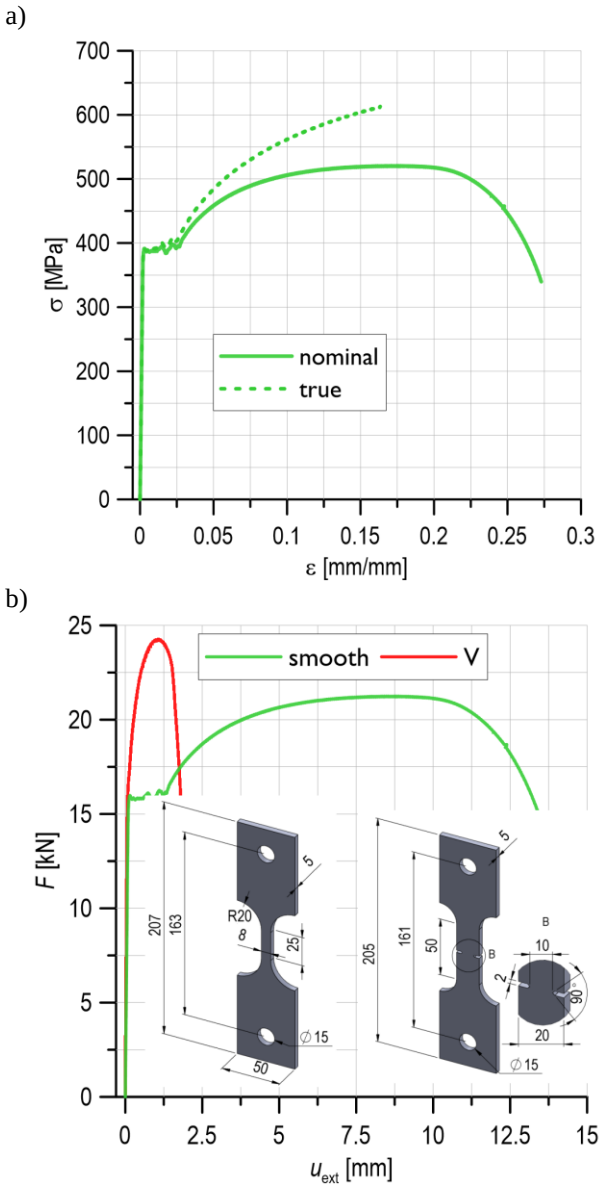

Fig. 2. Experimental results: a) nominal and true stress-strain relationship, b) the dependences of load-displacement and schematics of the specimens analysed

3. Numerical modeling and load simulations

The data recorded during the experimental tests served as the basis for the numerical tests. 3D modelling of the specimens, simulation loading and calculations were carried out in Abaqus ver. 6.12-2.

Numerical models of specimens identical to those used in the experimental studies were developed. Using symmetry, ¼ of each specimen was modelled. This allowed the number of nodes in the model to be reduced and the loading time to be reduced. An 8-node, three-dimensional finite element (type C3D8R) was used to build the mesh. In the numerical models, the mesh was compacted as it approached: the modelled notch (V-notch specimen) or the center surface (smooth specimen). The choice of finite element size and mesh densification variation were preceded by preliminary tests to obtain convergence of the results obtained. The smooth specimen model was divided into 6048 finite elements and the V-notched specimen model into 9642 finite elements. The boundary conditions assumed:

- on the wall perpendicular to the *Y* axis: blocking of displacements in the *Y* direction and rotation in the *X* and Z directions;
- on the wall perpendicular to the *X* axis: blocking of displacements in the *X* direction and rotation in the *Y* and *Z* directions;
- on the wall along the *Z* axis: blocking of displacements in the Z direction, rotation in the *X* and Y directions (Fig. 3).

The loading was simulated by means of a displacement of the end of the specimen in the *Y*-axis direction, whose values were set identical to the experimental ones. Stress and strain values were recorded at characteristic points in the loading diagrams (yield stress, $0.5(\sigma_{YS}+\sigma_{UTS})$, F_{max}, in the middle of neck formation, just before failure).

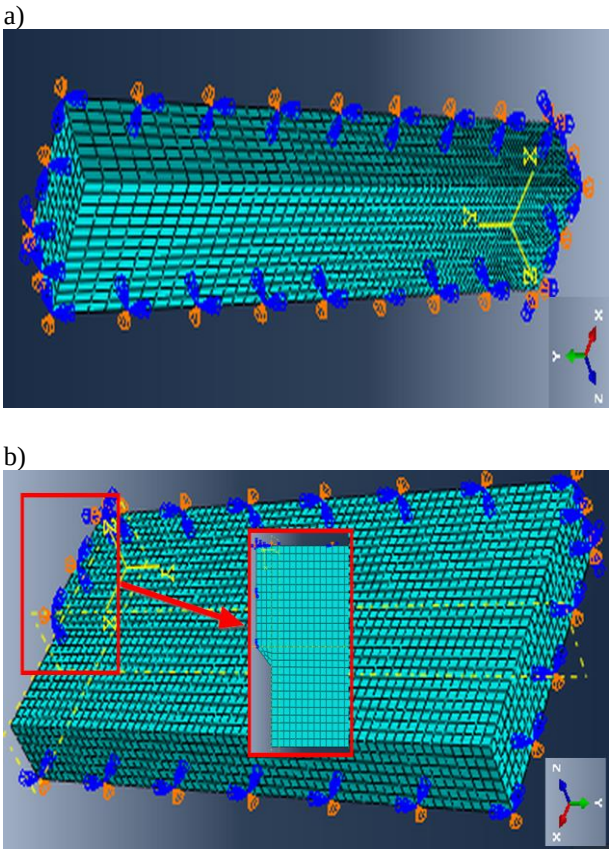

Fig. 3. Numerical specimen models: a) smooth, b) V-notched

A very important aspect in the preparation of numerical models of elements is the development and application of the correct material model- the true stress-strain relationship (constitutive relationship). Particular attention should be paid when analyzing a material with a significant level of ductility and when there are local sources of stress concentration (e.g. occurrence of notches). In the work of Wierzbicki, Bai, Bao et al. (Bai and Wierzbicki, 2008; Bao and Wierzbicki, 2004; Cravero and Ruggieri, 2007; Wierzbicki et al., 2005) and Neimitz and co-workers (Neimitz et al., 2018), a procedure for calibrating a material compound using a plasticity function was proposed. This function characterizes a curve that is located between contours in the deviator plane, in the principal stress space. The contours are derived from the assumptions of the strength hypotheses: Huber-von Mises (circle) and Tresca (hexagon) (Perić and Neto, 1999). In the proposed procedure, the size distributions of the numerically determined: stress components, strains, the stress triaxiality parameter and the Lode parameter are taken into account. For highly ductile materials, it is particularly important to introduce the material weakening determinant term proposed by Neimitz and co-workers (Neimitz et al., 2018). The introduction of a calibration of the constitutive relationship with the weakening term allows a very good agreement between the force-extension curve obtained experimentally and that determined numerically.

When defining the true stress-strain relationship from a uniaxial tension diagram, two sections are considered- the section where the material deforms uniformly and the section where neck formation takes place. The first section contains the elastic deformation and plastic sections, where the true stresses are calculated from the nominal ones according to the formulae:

$$\varepsilon_t = \ln(1 + \varepsilon_{nom}) \tag{1}$$

$$\sigma_t = \sigma_{nom}(1 + \varepsilon_{nom}) \tag{2}$$

The elastic part of the material model is defined by the values of Young's modulus and Poisson's ratio. For materials with a significant level of ductility, it is additionally required to determine the critical stress and strain values. The critical strain level of a material was estimated by measuring the elongation of ferrite grains in a smooth tensile specimen at ~275% (Dzioba and Lipiec, 2019). The true stress-strain relationship at the neck forming section was presented as a power law (see Fig. 4a), the parameters of which were selected iteratively, aiming for the best agreement between the experimental and numerical load curves (force-elongation) (Fig. 4b). When good agreement between the load curves was achieved, the material model was considered to provide valid results for the numerical simulations. Details on the methods used to define the material model for numerical calculations are presented in (Bucchi et al., 2022; Neimitz et al., 2018).

a)

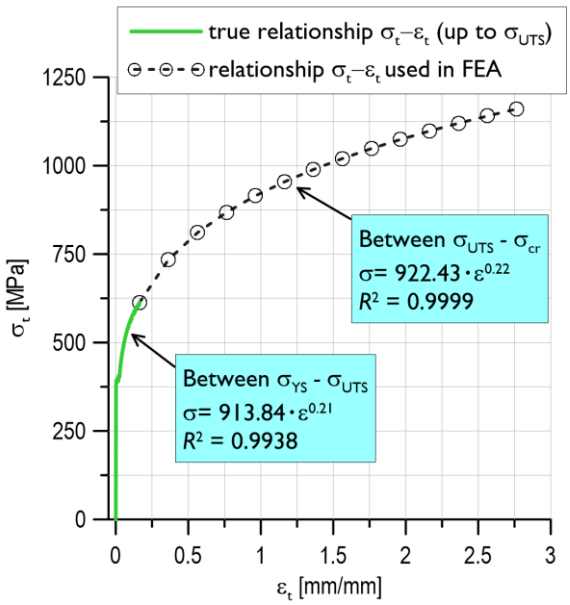

b)

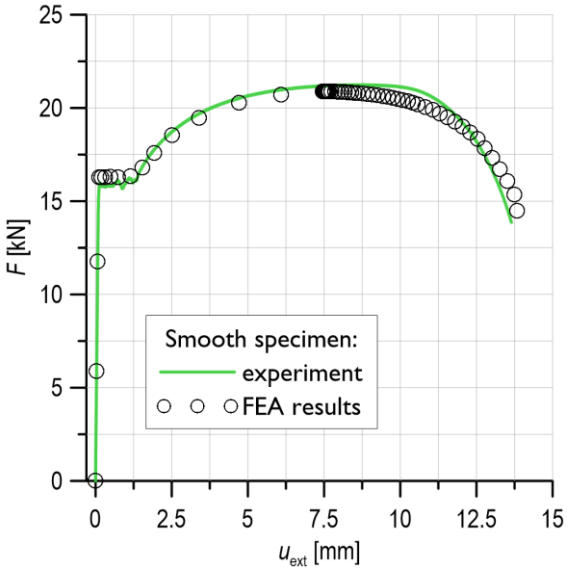

Fig. 4. Preparation of the material model for numerical calculations: a) true relationships, b) experimental and numerical load curves for the smooth specimen

4. Results and discussion

As a result of the numerical calculations carried out, the stress and strain fields occurring in the material of the specimens analyzed were determined.

Figures 5a and 5b show maps of the distributions of the stress components. Figures 6a and 6b show the strain components for the loading stage at which advanced neck development occurs. Figures 8a and 8b show the max values of the stress components at different loading stages of the specimens.

According to the maps of the stress tensor component σ_{22} (in the tensile direction), a higher stress level is appropriate for the smooth specimen compared to the V-notched specimen.

At fracture, the max values reach 1400 and 1000 MPa, respectively. In the smooth specimen, the maximum σ_{22} values occur in the central part of the plane of maximum constriction, while in the V-notched specimen they occur at the plane of maximum constriction at the apex of the notch.

From the maps for the stress component σ_{12}, it can be seen that their maximum values are located at some distance from the plane of greatest constriction and in the central part of the specimen. It should be noted that the σ_{12} values for the V-notched specimen reach much higher levels than in the smooth specimen (Fig. 5).

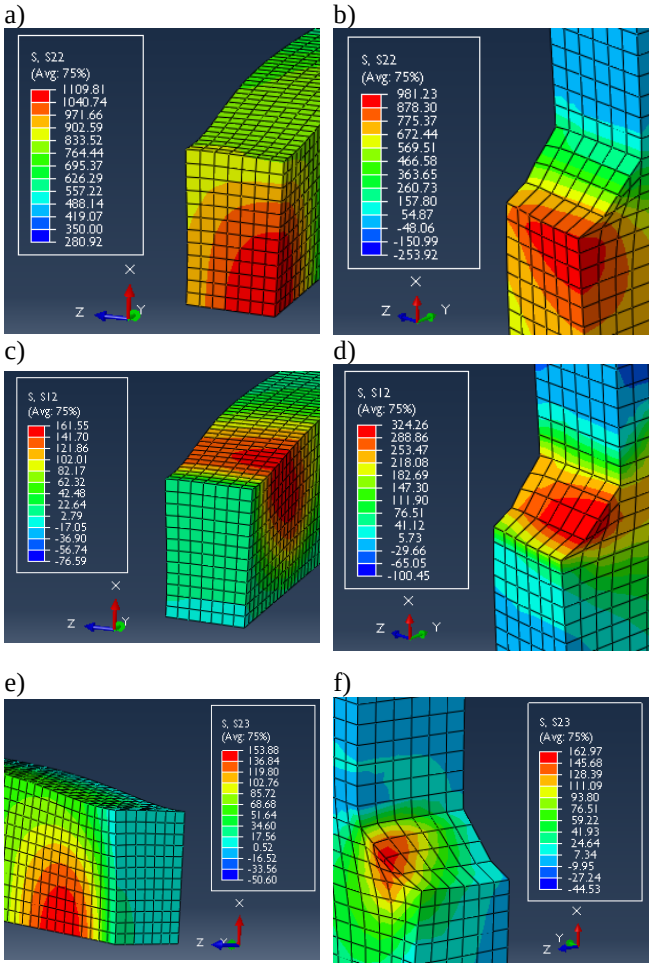

Fig. 5. Numerically determined fields of the individual components of the stress tensor for the specimens (at load prior to failure), smooth: a) σ_{22}, c) σ_{12}, e) σ_{23}, V-notch: b) σ_{22} , d) σ_{12}, f) σ_{23}

In the V-notched specimen, σ_{12} values ranging from 220 to 345 MPa were recorded immediately after plasticization and during plastic strain. In the smooth specimen, however, σ_{12} values did not exceed 192 MPa during plastic deformation until failure. Only just before failure did σ_{12} values reach 340 MPa.

For the σ_{23} component, the maximum values also occur at some distance from the plane of maximum constriction and at the outer (lateral) surface of the specimen. The σ_{23} values do not exceed the 192 MPa level when both specimens are loaded over the entire loading interval.

A value of 192 MPa was adopted in the quality of the reference level based on Tresca stress hypothesis. According to this hypothesis, plasticization of the material will occur when the value of the maximum shear stresses exceeds a limit value (denoted as k), defined as half of the yield stress value determined in a uniaxial tensile test. So, in a V-notched specimen, there should be a large amount of plasticization due to the stress σ_{12}.

Figures 6 show the strain maps of the specimens for pre-failure loading of the specimen. For the smooth specimen, the effective strain and ε_{22} are similar, their max values ($\varepsilon_{22} = \varepsilon_{eff} = 1.36$) are located in the central part of the plane of greatest constriction. This is twice as high as in the V-notched specimen ($\varepsilon_{eff} = 0.65$). Max strain values ε_{12} occur at some distance from the plane of greatest constriction and reach level $\varepsilon_{12} = 0.83$. For the V-notched specimen, the maximum values of the components of the strain tensor are located at the apex of the notch, but not at the plane of greatest constriction, but at the surface of the notch. The largest values were recorded for the tangential component $\varepsilon_{12} = 0.74$.

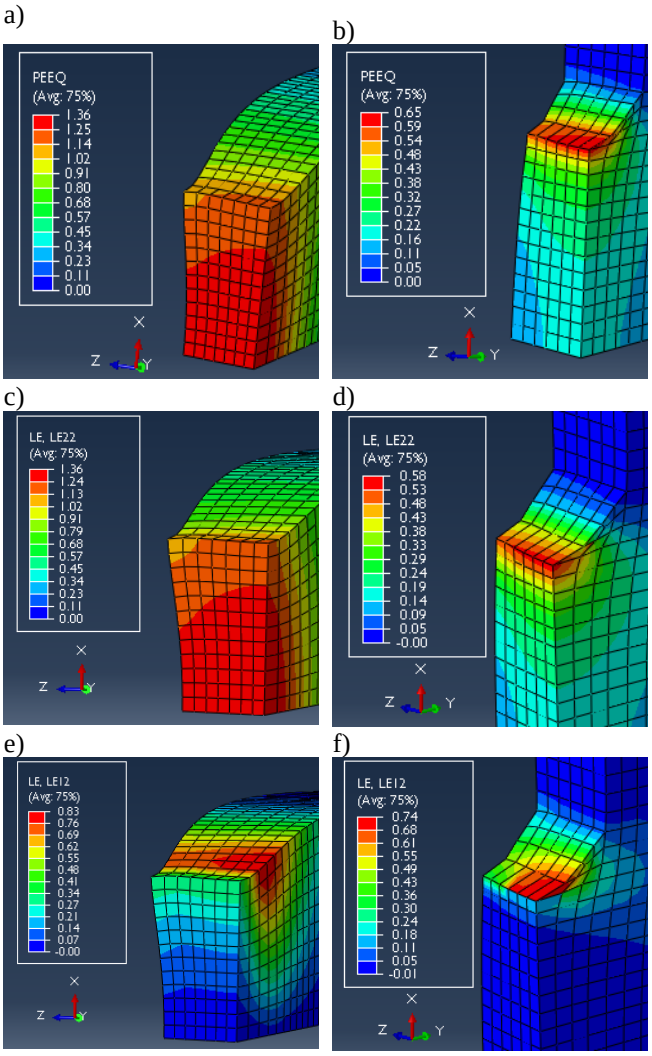

Fig. 6. Numerically determined distributions of strain components for the specimens (at load prior to failure), smooth: a) effective strain, c) ε_{22}, e) ε_{12}, V-notch: b) effective strain , d) ε_{22}, f) ε_{12}

The nature of the stress and strain component distributions in the analyzed specimens influences their fracture process (Fig. 7). In the smooth specimen, we observe the classical nature of fracture - in the central part there is a "bottom" area where fracture was realized due to the interaction of the normal component of the stress-strain tensor. In the zones near the lateral surfaces of the specimen, failure is realized through the interaction of tangential (Fig. 7b).

a)

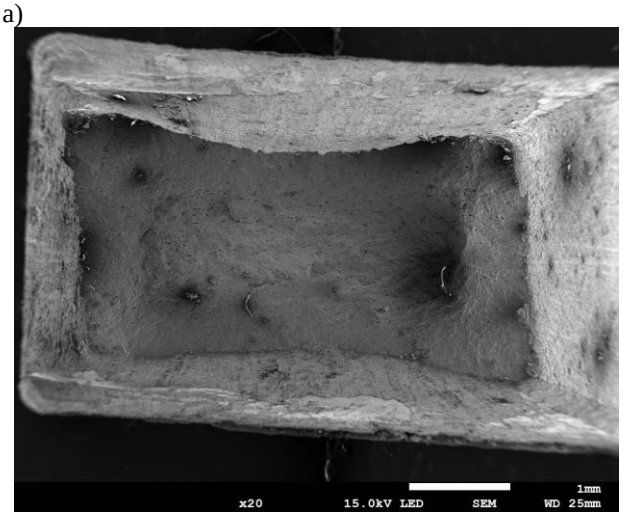

b)

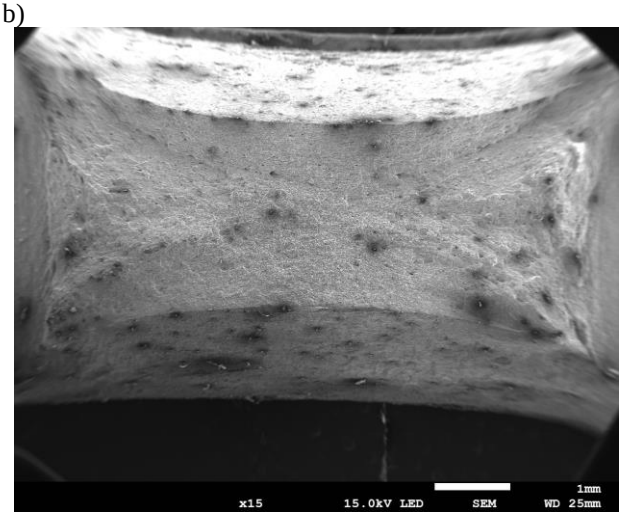

Fig. 7. The breakthroughs of the test specimens: a) smooth, b) V-notched

In the V-notched specimen, the level of the normal stress component σ_{22} is below the critical level (σ_{22} = 981 < σ_{cr} = 1160) (Fig. 8), so failure will not be realized. In contrast, during plasticization there is a high level of the tangential stress component σ_{12} significantly exceeding the reference level according to the Tresca's criterion ([σ]= 192 MPa). This implies a high development of plastic strain, resulting in the development of failure according to the slip shear mechanism (Fig. 8b).

a)

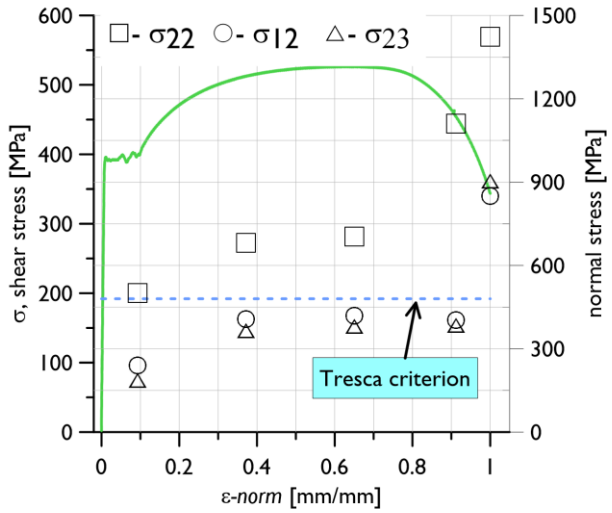

b)

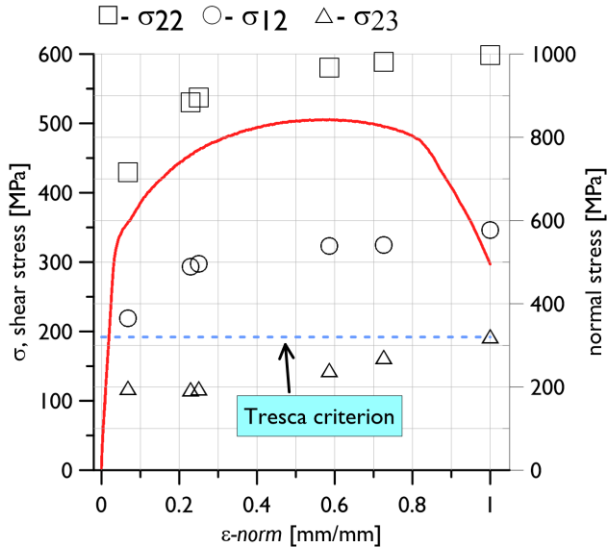

Fig. 8. Numerically determined shear and normal stress values with relation to normalized nominal strains for specimens: a) smooth, b) V-notched

5. Summary and conclusions

This paper presents the results of experimental tests and numerical calculations on the effect of the introduction of a sharp V-shaped notch on the failure process of a uniaxially tensile specimen. As a result of the analysis of the numerically determined stress and strain component fields in the vicinity of the plane of maximum specimen constriction, the conclusions presented below were established.

- In the smooth specimen, the highest values were obtained for the normal component of the stress, which is located in the central part of the plane of maximum specimen constriction and reaches the value σ_{22} =1400 MPa, which exceeds the value of the critical stress σ_{cr} =1160 MPa assumed in the material model. So the failure of the smooth specimen will start in the central zone of the plane of greatest constriction due to the normal component of the stress.

Then, in the areas near the lateral surfaces of the specimen, destruction will be realized by the action of the tangential components of stress.

- In the notched specimen, the maximum value of the normal component does not reach the critical value ($\sigma_{22} = 981 < \sigma_{cr} = 1160$). On the other hand, during the entire plasticization interval there is a high level of the stress component σ_{12}, which significantly exceeds the reference value according to the Tresca's criterion ($\sigma_{12} > [\sigma]$), and in the neck-forming section the values of σ_{12} almost double $[\sigma]$. So the destruction of the notched specimen starts due to the interaction of the σ_{12} component.
- Confirmation of the above conclusions is provided by the breakthroughs of the specimens. In the smooth specimen, the breakthrough consisted of a 'bottom' area and inclined lateral faces (Fig. 7a). In the V-notched specimen, there is no 'bottom' area, only inclined planes.

The results presented here were obtained in order to carry out further research on the assessment of the metal condition of the pipelines of the gas network of the Polska Spółka Gazownictwa (PSG). This research used the recording and analysis of acoustic emission (AE) signals. The results presented in this paper were used to establish relationships between characteristic types of AE signals and pipeline material destruction processes. The results of this research will be presented in the next article.

Acknowledgements

The work was created as part of the project entitled "Sildig AE - System for Identifying and Locating Gas Infrastructure Defects Using the Acoustic Emission Method" co-financed by the European Regional Development Fund under Sub-measure 1.1.1 of the Intelligent Development Operational Program 2014-2020, contract no. POIR.01.01.01- 00-1019/19-00 of June 10, 2020. The project was carried out in a consortium by Polska Spółka Gazownictwa sp.z o.o. (Polish Gas Distribution Group - Consortium Leader) and Kielce University of Technology (Consortium Member).

Reference

Alzyod, H., Ficzere, P. 2023. Correlation Between Printing Parameters and Residual Stress in Additive Manufacturing: A Numerical Simulation Approach . Production Engineering Archives, 29(3), 279-287. DOI: 10.30657/pea.2023.29.32

ASTM E8 / E8M-16ae1, 2016. ASTM E8 / E8M-16ae1, Standard Test Methods for Tension Testing of Metallic Materials. ASTM International, West Conshohocken.

Bai, Y., Wierzbicki, T., 2008. A new model of metal plasticity and fracture with pressure and Lode dependence. International Journal of Plasticity 24, 1071–1096. DOI: 10.1016/j.ijplas.2007.09.004

Bao, Y., Wierzbicki, T., 2004. On fracture locus in the equivalent strain and stress triaxiality space. International Journal of Mechanical Sciences, 46, 81–98. DOI: 10.1016/j.ijmecsci.2004.02.006

Benhamena, A., Fatima, B., Foudil, K., Baltach,, Chaouch, M. 2023. Numerical analysis of fracture behavior of functionally graded materials using 3D-XFEM. Advances in Materials Science, 23(3), 33-46. DOI: 10.2478/adms-2023-0015

Bokůvka, O., Jambor, M., Trško, L., Nový, F., Lisiecka, B., 2018. Fatigue lifetime of 20MnV6 steel with holes manufactured by various methods. Production Engineering Archives 19, 3–5. DOI: 10.30657/pea. 2018.19.01

Bucchi, F., Frendo, F., Moreschini, C., 2022. Influence of the stress history and of the Lode angle on the determination of the ductile fracture locus for two steel alloys. Engineering Fracture Mechanics 274, 108759. DOI: 10.1016/j.engfracmech.2022.108759

Castillo, C., Fernandez, V., Lordan, O., 2021. A Markovian-based simulation model for the evolution of employees' emotional states during an organizational change. Polish Journal of Management Studies, 23(1), 119-135. DOI: 10.17512/pjms.2021.23.1.08

Cravero, S., Ruggieri, C., 2007. Estimation procedure of J-resistance curves for SE(T) fracture specimens using unloading compliance. Engineering Fracture Mechanics 74, 2735–2757. DOI: 10.1016/j.engfracmech. 2007.01.012

Dzioba, I., Lipiec, S., 2019. Fracture Mechanisms of S355 Steel–Experimental Research, FEM Simulation and SEM Observation. Materials, 12, 3959. DOI: 10.3390/ma12233959

Fan, W., Yang, H., Taylor, A.C., 2023. Numerical analysis of fracture in interpenetrating phase composites based on crack phase field model, Composites Science and Technology, 232, 109873, DOI: 10.1016/j.compscitech.2022.109873.

Fonzo, A., Meleddu, A., Di Biagio, M., 2006. Crack propagation modeling and crack arrestor design for X120. International Pipeline Conference, 317-325. DOI: 10.1115/IPC2006-10319

Gumen, O., Ujma, A., Kruzhkova, M., 2021. Research into the process of spraying complex titanium and zirconium nitride on structural steel and reaction times relating to the final finish and quality obtained. BoZPE 10, 71–76. DOI: 10.17512/bozpe.2021.1.07

Jian, S., Hong, Z., Kui, X., 2004. Numerical simulation of dynamic cracks propagation in gas transmission pipeline. Oil and Gas Storage and Transportation, 23, 5–8.

Karkowski, M., Grondys, K., 2021. Performance Assessment of Balance Algorithm Based Motorway Car Park Occupancy Information System. Polish Journal of Management Studies, 24(2), 178-193. DOI: 10.17512/pjms.2021.24.2.11

Kosiń, M., Pawłowski, K., 2017. Numeryczna analiza złącza przegrody zewnętrznej wykonanej w technologii szkieletowej. BoZPE, 19, 111–120. DOI: 10.17512/bozpe.2017.1.16

Misawa, K., Imai, Y., Aihara, S., 2011. A New Model for Dynamic Crack Propagation and Arrest in Gas Pipelines. Presented at the 2010 8th International Pipeline Conference, American Society of Mechanical Engineers Digital Collection, 685–694. DOI: 10.1115/IPC2010-31475

Mitsuya, M., Motohashi, H., Oguchi, N., Aihara, S., 2013. Calculation of Dynamic Stress Intensity Factors for Pipes During Crack Propagation by Dynamic Finite Element Analysis. Journal of Pressure Vessel Technology, 136. DOI: 10.1115/1.4025617

Neimitz, A., Gałkiewicz, J., Lipiec, S., Dzioba, I., 2018. Estimation of the onset of crack growth in ductile materials. Materials, 11, 1–19.

Parlak, B.O., Yavasoglu, H.A., 2023. A Comprehensive Analysis of In-Line Inspection Tools and Technologies for Steel Oil and Gas Pipelines. *Sustainability*, 15(3):2783. DOI: 10.3390/su15032783

Perić, D., Neto, E.A. de S., 1999. A new computational model for Tresca plasticity at finite strains with an optimal parametrization in the principal space. Computer Methods in Applied Mechanics and Engineering, 171, 463–489. DOI: 10.1016/S0045-7825(98)00221-7

Piątkowski, J, Gajdzik, B, Mesjasz, A., 2020, Assessment of Material Durability of Steam Pipelines Based on Statistical Analysis of Strength Properties–Selected Models. *Energies*, 13(14), 3633. ttps://doi.org/10.3390/en13143633

PN-EN ISO 6892-1:2020-05, 2019. PN-EN ISO 6892-1:2020-05, Metallic materials – Tensile testing – Part 1: Method of test at room temperature. International Organization for Standardization, Geneva.

Sharma, V.B,, Singh, K., Gupta, R., Joshi, A., Dubey, R., Gupta, V., Bharadwaj, S., Zafar, M.I, Bajpai, S, Khan, M.A,, et al. 2021, Review of Structural Health Monitoring Techniques in Pipeline and Wind Turbine Industries. *Applied System Innovation*, 2021; 4(3), 59. DOI: 10.3390/asi4030059

Song, J.-H., Belytschko, T., 2009. Dynamic Fracture of Shells Subjected to Impulsive Loads. Journal of Applied Mechanics 76. DOI: 10.1115/1.3129711

Świt, G., Dzioba, I., Adamczak-Bugno, A., Krampikowska, A., 2022. Identification of the Fracture Process in Gas Pipeline Steel Based on the Analysis of AE Signals. Materials, 15, 2659. DOI: 10.3390/ma15072659

Wierzbicki, T., Bao, Y., Lee, Y.-W., Bai, Y., 2005. Calibration of seven fracture models. International Journal of Mechanical Sciences, 47, 719–743.
Xiaobin, Y., Zhuang, Z., Chuan Jing, Z., 2008. Numerical Simulation on dynamic crack extension of rich gas transmission pipeline. Journal of Tsinghua University: Natural Science Edition, 48, 1355–1358.
Zhao, M.-C., Yang, K., Shan, Y., 2002. The effects of thermo-mechanical control process on microstructures and mechanical properties of a commercial pipeline steel. Materials Science and Engineering, 335, 14–20. DOI: 10.1016/S0921-5093(01)01904-9

光滑和凹口V形试样断裂过程的实验数值分析

關鍵詞
管道
有限元法
应力
应变
特雷斯卡准则

摘要
本文介绍了对从天然气输送管道中提取的经单向张力加载的光滑和V凹槽试样进行的质量测试的结果。V凹槽的引入导致了在最大收缩平面附近的应力和应变分量场的变化，从而导致它们通过不同的机制发生破裂。该过程包括实施质量管理实践，如使用ABAQUS对试样进行数值建模和模拟加载。在这些计算中采用的材料模型经过定义和验证，以确保质量控制。在数值计算之后，生成了应力和应变分量场的图表，有助于对试样的质量评估。结果表明，对于光滑试样的质量管理过程主要是由于最大收缩平面的中心区域中的法向应力分量引发了破裂的初期。相反，在V凹槽试样中，质量管理工作揭示了由于切应力分量引发了破裂的初期，然后通过剪切机制进行了破裂。这些结果对于制定一个基于声发射信号分析的质量驱动的方法，以监测天然气管道的运行安全，具有重要价值